



# Mapping tropical forest trees across large areas with lightweight cost-effective terrestrial laser scanning

Shengli Tao<sup>1</sup> · Nicolas Labrière<sup>1</sup> · Kim Calders<sup>2</sup> · Fabian Jörg Fischer<sup>1</sup> · E-Ping Rau<sup>1</sup> · Laetitia Plaisance<sup>1</sup> · Jérôme Chave<sup>1</sup>

Received: 27 February 2021 / Accepted: 29 October 2021 / Published online: 28 December 2021  
© INRAE and Springer-Verlag France SAS, part of Springer Nature 2021

## Abstract

• **Key message** We used lightweight terrestrial laser scanning (TLS) to detect over 3000 stems per hectare across a 12-ha permanent forest plot in French Guiana, 81% of them < 10 cm in trunk diameter. This method retrieved 85% of the trees of a classic inventory. Finally, TLS revealed that stem positions of the classic inventory had geolocation errors of up to 6 m.

• **Context** Accurate position mapping of tropical rainforest trees is crucial for baseline studies of tropical forest ecology but is labor-intensive. Terrestrial lidar scanning (TLS) is broadly used in temperate forest inventories, but its use in rainforests is restricted to the determination of individual tree volumes within small survey areas.

• **Aims** Mapping tree stems across one large (12-ha) rainforest plot, including trees less than 10 cm DBH, and evaluating the precision of traditional mapping approaches.

• **Methods** We used lightweight TLS, co-registered the acquisitions, and developed a new efficient algorithm to process the TLS data.

• **Results** We detected 36,422 stems of which 29,665 (81%) were < 10 cm in diameter at breast height (DBH). Of the trees ≥ 10 cm DBH previously censused in the plot, 85% were identified by TLS. Automatic DBH estimation from TLS data had an RMSE of 6 cm. RMSE was improved to 3 cm by a manual verification of the shape and quality of the stem points. The initial census map had substantial bias in tree geolocation with a maximum value around 6 m.

• **Conclusion** Lightweight TLS technology is a promising tool for the estimation of stem tapering and volume. Here, we show that it also facilitates the establishment of large tropical forest inventories, by improving the positioning of trees, thus increasing the accuracy of forest inventories and their cost-effectiveness.

**Keywords** Forest inventory · Amazon forest · Nouragues · Terrestrial Lidar · Topography · Stem diameter

---

**Handling Editor:** John M Lhotka

---

✉ Shengli Tao  
sltao1990@gmail.com

✉ Jérôme Chave  
jerome.chave@univ-tlse3.fr

Nicolas Labrière  
nicolas.labriere@gmail.com

Kim Calders  
Kim.Calders@ugent.be

Fabian Jörg Fischer  
Fabian.J.D.Fischer@gmx.de

E-Ping Rau  
epingchris@gmail.com

Laetitia Plaisance  
laetitia.plaisance@univ-tlse3.fr

<sup>1</sup> Laboratoire Évolution Et Diversité Biologique, UMR 5174 (CNRS/IRD/UPS), 31062 Toulouse Cedex 9, France

<sup>2</sup> CAVELab - Computational & Applied Vegetation Ecology, Faculty of Bioscience Engineering, Dept. of Environment, Ghent University, Ghent, Belgium

## 1 Introduction

Tropical rainforests harbor a high biological diversity and store large amounts of carbon (Hubbell 2001; Pan et al. 2011). Documenting the position and size of every tropical forest tree in a reference area (i.e., forest inventory) is fundamental for any baseline studies of tropical ecology and ecosystem modeling (Brienen et al. 2015; Visser et al. 2016; Clark et al. 2017). Ground-based forest inventories are useful for the detection of changes in carbon storage and shifts in population densities (Chave et al. 2019). However, the monitoring of trees in structural complex forest communities such as tropical rainforests is time-consuming and labor-intensive.

The traditional approach to mapping rainforest trees is through the establishment of permanent forest plots. The size of the plot is typically 100×100 m, but sometimes larger. Plot establishment protocols recommend to grid the plot at 10×10 m or 20×20 m resolution, within which each stem is tagged and mapped visually relative to the position of the subplot corners. If the subplot is accurately established, then trees can be positioned with metric accuracy across the entire plot (Condit 1999; Phillips et al. 2010). However, the establishment of a grid with topographic variation accounted for requires a considerable time investment, and ideally requires total stations, but is generally based on traditional surveying based on measuring tapes. Because of the complex terrain, tree positioning may thus be error prone, meaning that the geolocation of trees as reported in forest inventories may be quite different from their true position.

By capturing the 3D structure of a forest understory at millimetric resolution, terrestrial laser scanning (TLS) has opened up many possibilities in forest ecology (Calders et al. 2015; Newnham et al. 2015; Malhi et al. 2018; Disney et al. 2018; Disney 2019; Brede et al. 2019; Lau et al. 2019). Stem mapping is an obvious application of TLS (Newnham et al. 2015), and TLS has been routinely used to map stems in

boreal and temperate forest plots (Maas et al. 2008; Yao et al. 2011; Tao et al. 2015; Liang et al. 2018). However, the stem mapping procedures developed for boreal and temperate forests cannot be easily applied to tropical rainforests, where stem density and under-canopy structural complexity can be much higher. As a result, most applications with TLS in tropical forests have been conducted to reveal the architecture of large trees (Wilkes et al. 2017; Raunonen et al. 2013; Burt et al. 2019; Martin-Ducup et al. 2021). For example, Burt et al. (2019) completed 121 acquisitions in a 1-ha plot with a RIEGL VZ-400 instrument, and they reconstructed the full 3D architecture of many large trees in the plot. Momo Takoudjou et al. (2018) reconstructed 61 large trees in the tropical forests of Cameroon using a Leica C10 Scanstation, and Gonzalez de Tanago et al. (2018) used a RIEGL VZ-400 to scan 29 large trees in Guyana. While large trees contribute most to the above ground biomass of rainforest, small trees with a diameter at breast height (DBH) < 10 cm contribute disproportionately to the understory stand structure and are essential for biodiversity and long-term monitoring of the forest. One key challenge is that it is more difficult to detect smaller trees automatically in TLS data due to the signal-to-noise ratio. In addition, commonly used long-range time-of-flight TLS systems, such as the RIEGL VZ series, are relatively heavy (~ 10 kg), making it difficult to acquire high-quality scans over several hectares of forest (Wilkes et al. 2017). Here, we seek to assess the potential for lightweight TLS systems to map large plots in heterogeneous tropical rainforests, and to overcome the joint challenges of large area scanning and small tree detection.

Lightweight TLS is a recent advance in TLS technology (Bauwens et al. 2016; Brede et al. 2017; Qian et al. 2017). These lightweight scanners tend to have a reduced range compared to long-range scanners (Calders et al., 2020), but are sufficient for many applications. The Leica BLK360 scanner (~ 1 kg, Table 1) has been tested for 3D architecture reconstruction of large tropical trees (Disney et al. 2019)

**Table 1** Specifications of the BLK360 terrestrial laser scanner

Weight	~ 1 kg
Height/diameter	16.5/10 cm
Effective range	0.6–60 m
Accuracy	7 mm at a distance of 20 m
Beam divergence	0.4 mrad
Point measurement rate	Up to 360,000 points per second
Scanning mode	Low-, medium-, and high-point density scanning, with a point density at 7.5 m of 20×20, 10×10, and 5×5 mm, respectively
Horizontal/vertical field of view	360/300°
Camera	RGB camera, longwave thermal camera

For more information: <https://leica-geosystems.com/products/laser-scanners/scanners/blk360>

and detection of small tropical trees (5–10 cm DBH; Luck et al. 2020).

In the present study, we aimed at cost- and time-effective large-area scanning and high stem detection rate, with a focus on accurate positioning of rainforest trees using the BLK360. Many plots, even those established decades ago and regularly re-censused, have errors in stem positioning. We developed a sampling scheme suitable for large area scan acquisition and efficient data merging with the lightweight laser scanner (Text 1 in the Appendix). We also implemented a new method to detect a broad range of stem sizes from the acquired point cloud. A high-resolution digital terrain model (DTM) was built based on these data and it was compared with a previously acquired airborne Lidar product. Finally, DBHs of the detected stems were estimated and compared with ground measurements. Although TLS provides rich 3D structural information on tree architecture, DBH is a key metric for forest inventory. We expect that lightweight cost-effective TLS is capable of mapping stems more efficiently than classic inventories.

## 2 Materials and methods

### 2.1 Data acquisition

Fieldwork was conducted in October 2019 at the Nouragues Ecological Research Station (4° 05' N, 52° 40' W; [www.nouragues.cnrs.fr](http://www.nouragues.cnrs.fr)), French Guiana. The study area is covered by a closed-canopy tropical forest, and it has a mean rainfall of 2900 mm/year, with a dry season from late August to

mid-November, and a shorter dry season in March (Chave et al. 2008). The area is nested within a Natural Reserve and is free from any recent human disturbance or encroachment.

The permanent plot, called “Petit Plateau,” covers 12 ha (400 × 300 m) and has been established in 1994. In 2012, a 20-m grid system was established inside the plot using tapes and handheld compasses. All stems ≥ 10 cm DBH have been mapped and tagged (Chave et al. 2008), with tree species identification conducted in 2010–2012. The site has been re-censused in 2001, 2007, 2012, and 2017.

The full plot was scanned using two BLK360 laser scanners simultaneously, to halve acquisition time. Scanner specifications are listed in Table 1. We performed one scan at every 20 m on the grid nodes, with scan mode set to high point density (Fig. 1), to balance survey efficiency with data accuracy. In very few cases where heavy occlusion effects were encountered based on visual assessment, we added a middle scan at a 10-m distance from the previous one. To co-register the individual scan acquisitions, we used five sets of 12-cm spherical targets. The targets were purchased for less than 5€ each (Fig. 1c). Two sets of targets (light and dark blue in Fig. 1a) were displaced along the scan trajectory, linking the current scan (black dot in Fig. 1a) to the previous and next ones. The three other sets of targets were placed between scan lines and used as reference points to merge the scan lines, so as to minimize the cumulative error between adjacent scan lines (see Text 1 in the Appendix for further details). A total of 395 scans were acquired across the 12-ha plot. To co-register individual TLS scans, the spherical targets were automatically recognized by the Leica Cyclone Register 360 software, with little need for

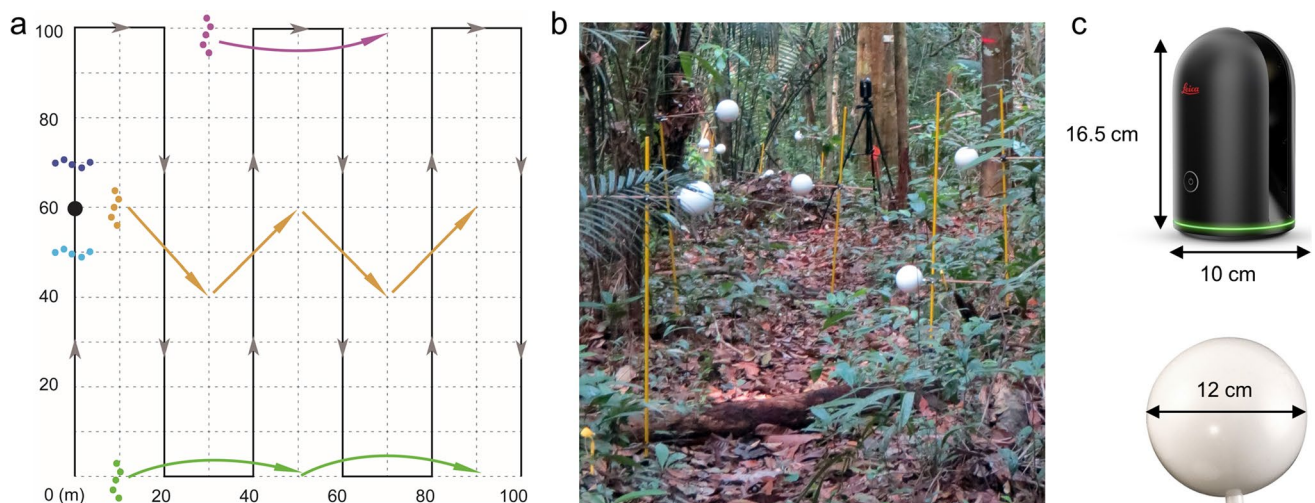


**Fig. 1** Scanning of a tropical rainforest patch with a BLK360 terrestrial laser scanner. **a** “Continuous chain” sampling design with a 20-m-gridded scanning, illustrated in a 1-ha area. The gray arrows indicate the progress of the scanning, with the current scan location shown as a black dot. Five target sets, each having five targets, were

used in total and are represented as colored dots. **b** Photograph of the scanner and targets placed in the field (credit: E-Ping Rau). **c** Close-up images for the lightweight scanner and targets. See Appendix-Text 1 and Fig. 18 in the Appendix for more information on how the targets were displaced with the laser scanner

manual adjustments. The size of the final dataset was ~ 500 Gigabytes (Gb) in “las” format.

## 2.2 High-resolution digital terrain model

Prior to stem mapping, we identified the ground points and built a high-resolution digital terrain model (DTM) (see Text 2 in the [Appendix](#) for a step-by-step instruction on data processing). We first extracted the lowest point in each  $10 \times 10$  cm tile using the Lastools software (lastools.org) to reduce the computational burden. We then extracted the ground points by calculating the minimum height difference between neighboring pairs and excluding those  $\geq 50$  cm above their neighbors (Fig. 9 in the [Appendix](#)). The filter was implemented in Matlab R2018b (MathWorks Inc) and the runtime was ~ 50 min across the 12-ha area. A DTM was then created at 20-cm horizontal resolution using Quick Terrain Modeler (QTM) software. It was compared with a 1-m resolution DTM obtained in 2015 with airborne laser scanning at a ground point density of  $0.47 \text{ points m}^{-2}$  (Labrière et al., in preparation).

## 2.3 Stem mapping

Vegetation points were subsampled to achieve a pairwise distance  $\geq 2$  cm, to reduce the computational burden, in CloudCompare (danielgm.net/cc/). Point elevations were then recomputed relative to the DTM (“lasheight” routine). Seven height layers were defined: 0.5–1 m, 1–1.5 m, 1.5–2 m, 2–2.5 m, 2.5–3 m, 3–3.5 m, and 3.5–4 m. The lowest height layer (0.5–1 m) was used for detecting small trees close to the ground. To detect larger trees, we explored the height layers above 1.5 m. We calculated the surface normal direction for each point, that is, the vector direction perpendicular to the tangent plane of the surface at a point. Points with a normal direction  $90^\circ \pm 10^\circ$  from the vertical were assumed to belong to stems (referred to as “potential stem points”). A tolerance of  $10^\circ$  was allowed because some trees are inclined.

Some non-stem points may be falsely classified as potential stem points if the features are vertical (Fig. 2a). We filtered out these points by designing a filter referred to as the “tube filter.” For each potential stem point (black point in Fig. 2b), we placed a “tube” ( $10 \times 10$  cm in the  $xy$ -dimension) centered around it and searched for potential stem points across smaller bins immediately above and below it (Fig. 2b). Because stems could be insufficiently scanned (e.g., having no points in the top-most and bottom-most height layers), the tube’s vertical size was set adaptively. The tube filter removed many non-stem points (Fig. 2c). This was implemented separately on each of the five height layers to improve the detection rate of stem points (Fig. 2d).

The stem points detected from different height layers were then merged and segmented horizontally with a minimum distance of 10 cm between the segmented components (i.e., putative stem). Only the segmented components with a vertical span  $\geq 0.8$  m (in the 0.5–1.5 m height class) and  $\geq 1$  m (above 1.5 m) were retained, so as to exclude vertical branches. The influence of the parameters on stem detection is discussed below. The stem detection procedure was implemented in Matlab.

The segmentation described above assumed that stems had a pairwise distance  $> 10$  cm. Consequently, stems growing less than 10 cm apart would have been wrongly segmented as one stem. To correct this under-segmentation error, we assessed whether each stem could be further segmented using the DBSCAN algorithm, a density-based spatial clustering of applications with noise. We used the default parameters based on our point density (2 cm between-point distance; Ester et al. 1996; Fig. 10a in the [Appendix](#)). We also visually checked all stems  $\geq 50$ -cm trunk diameter (see below for diameter calculation), which are likely to be segmented into more than one component (over-segmentation error; Fig. 10b in the [Appendix](#)). Visual inspection took one person about 4 h for the 12-ha area. To quantify the rate of false positives (i.e., number of false stems), we selected five subregions in the four corners and center of the 12-ha plot (Table 2; Fig. 11 in the [Appendix](#)). In these five regions, TLS-detected stems were visually inspected against the raw point cloud to decide which stem was a false-positive error.

## 2.4 Stem diameter calculation

We calculated a proxy of trunk diameter by extracting the stem dimensions along both horizontal axes (referred to as the “ $xy$ -range” approach; Fig. 3a). Specifically, we calculated the average of  $x$ - and  $y$ -ranges every 10 cm along the vertical axis of each stem and took the median value as a final estimate of stem diameter — this method alleviates the influence of noisy points or missing stem points on DBH estimation and uncertainties in the estimated DBHs for leaning stems. The “ $xy$ -range” approach can be inaccurate for partially scanned stems or giant stems with buttresses or stilt roots, because we used the stem section from the ground to 4 m aboveground. We then also designed a semi-automatic approach for DBH estimation. The vertical principal axis of each stem (growth direction) was determined by a rotation, and the stem points were then projected to the plane perpendicular to the vertical principal axis. This ensures an accurate determination of DBH for leaning stems. We manually selected points of the stem’s outer region and fitted a circle if the stem was partially scanned (Pueschel et al. 2013; Fig. 3c), or calculated a diameter  $D$  from the basal area  $BA$  if the stem was irregularly shaped or buttressed:  $D = (4 BA/\pi)^{1/2}$  (Fig. 3b). The semi-automatic approach was

**Fig. 2** Automatic stem detection from TLS. **a** Stem points identified by surface normal calculation. Some leaf points were falsely identified as stem points. **b** The “tube filter” to filter out non-stem points. The tube filter was applied on each red point shown in **a**. **c** Stem points after the implementation of the tube filter. **d** Continuous detection of stem points at different height layers. Three layers (red, yellow, and blue) are shown here as examples

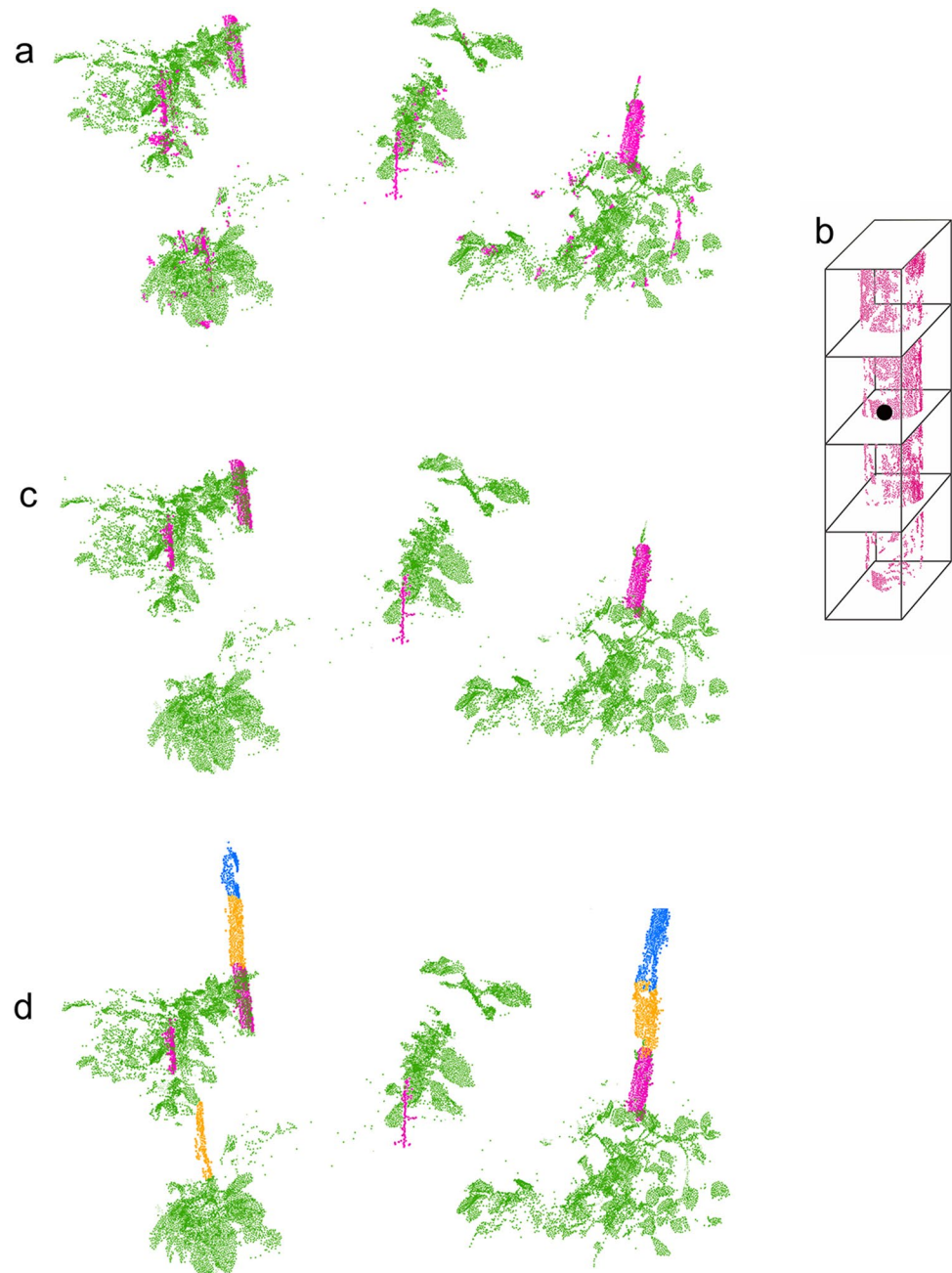
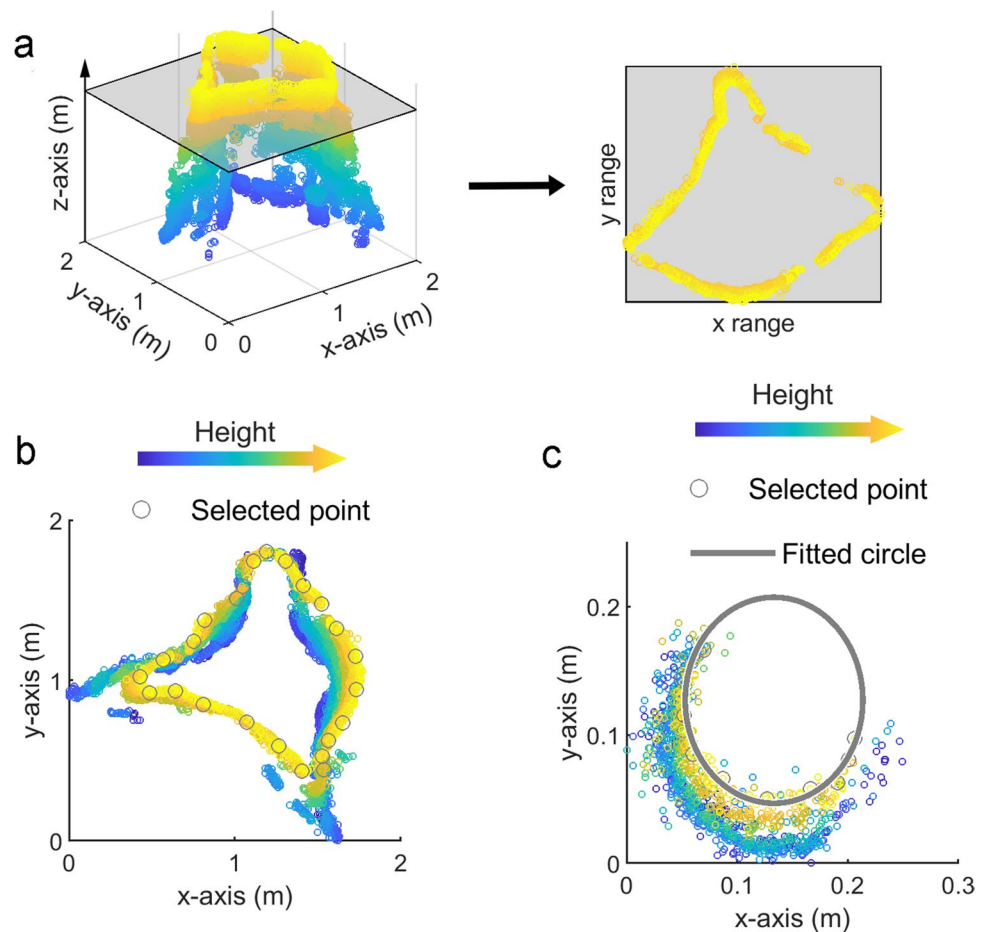


**Table 2** False-positive errors of the light TLS-detected stems in five regions of the 12-ha plot. See Fig. 11 in the [Appendix](#) for more information

Region	Size	Number of stems	Number of false-positive stems	False-positive rate (%)
Region 1 (plot center)	1415 m <sup>2</sup> (40×35 m)	575	22	3.8
Region 2 (upper left)	1480 m <sup>2</sup> (41×40 m)	337	12	3.6
Region 3 (lower left)	1480 m <sup>2</sup> (42×35 m)	386	15	3.9
Region 4 (upper right)	1272 m <sup>2</sup> (40×33 m)	286	11	3.8
Region 5 (lower right)	1444 m <sup>2</sup> (41×35 m)	463	20	4.3
All regions	7091 m <sup>2</sup>	2047	80	3.9

**Fig. 3** TLS-based DBH estimation. **a** The “xy-range” approach computing a surrogate of DBH:  $x$ - and  $y$ -ranges were measured and averaged every 10 cm along the  $z$  axis of each stem, and the median was used as a surrogate of stem diameter. **b** The semi-automatic approach of DBH estimation for large-sized trees. Border points on the stem cross-section were manually selected and basal area  $BA$  was estimated, then the stem diameter  $D$  was computed from the formula  $BA = \pi D^2/4$ . **c** Semi-automatic DBH estimation for insufficiently scanned stems. If possible, stem points were manually selected and a circle was fit to the points, resulting in an estimate of DBH



tested on five hundred randomly selected stems. For large stems (above 1 m DBH), trunk diameters were measured in the field at a tree-specific height to avoid the influence of buttress and stilt roots (Condit 1998; Cushman et al. 2021), but this height was not precisely recorded for all large stems. We therefore calculated their TLS-based diameters every 1 m along the  $z$  axis up to 13 m and selected the best match with field values.

## 2.5 Comparison between TLS-derived and field-censused stem maps

We compared the TLS-derived stem map against a field census of the Petit Plateau plot carried out in November 2017, ca. 2 years before the laser scanning campaign. During the census, the stems  $\geq 10$  cm DBH were manually geolocated relative to the subplot corners. These were compared with TLS-derived stem locations, calculated as the mean coordinates of the stem points. We visually paired TLS-derived and field-recorded stem geolocations. The process was seeded using large trees

for which locations could be unambiguously matched ( $\sim 1000$  trees), which were used as anchor points for further tree matching. To aid the process of stem pairing, we updated the position of each ground-censused stem based on triangulation of its nearby anchor points. If the updated position showed a high similarity with a TLS-derived stem, a new pair of anchor points was established. The visual pairing process was conducted within 1-ha subplots, then within  $1/4$ -ha subplots. This approach was repeated until no more trees could be matched with high confidence.

Using the visually paired geolocations, a bias map in tree geolocation was generated for the 12-ha plot. This was achieved by calculating the biases in positions of ground-censused stems along both the coordinates and interpolating the biases across the plot at 1-m resolution using nearest-neighbor interpolation.

Finally, we compared TLS-derived and field-recorded DBHs by plotting them against each other and calculating common measures of goodness-of-fit such as root mean square error (RMSE).

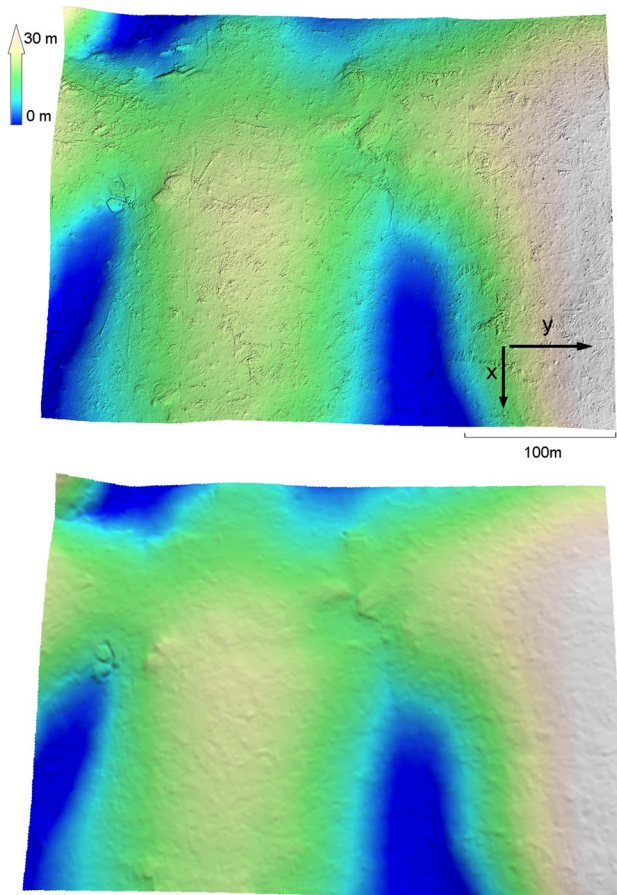


**Fig. 4** TLS-derived digital terrain model (DTM) at 0.2-m resolution (top) versus airborne Lidar-derived terrain model at 1-m resolution (bottom). Terrain elevation was normalized to have a minimum value of zero. For more information on DTM generation, see Fig. 9 and Text 2 in the [Appendix](#)

### 3 Results

Using two BLK360 instruments, 18 days of fieldwork and six persons were needed to complete the survey of the 12-ha plot (that is, about 10 person-days per ha). Post-processing of the 395 TLS scans (mainly stitching and subsampling) required ~3 days of lab work for one person using the Cyclone Register 360 software and CloudCompare. The stem detection procedure required 10 h of processing time using the newly developed Matlab routine.

Across the 12-ha plot, the TLS-based DTM had similar patterns compared with that inferred from airborne Lidar (Fig. 4), but captured more fine-scale variations of the terrain. For instance, the steep terrain in one corner of the plot was better captured by TLS than by airborne Lidar.

The stem mapping procedure detected 36,422 stems (Fig. 5). Of these, 29,665 (81%) had an inferred DBH < 10 cm. About 6% of the stems were under-segmented, and the DBSCAN procedure corrected this (Fig. 10a in the [Appendix](#)). About 120 large stems were visually confirmed as over-segmented, and this was manually corrected (Fig. 10b in the [Appendix](#)). The DBH-size distribution of the TLS-detected stems was log-normal, peaking around 3.5 cm (Fig. 5a). It follows that small trees less than about 4 cm in DBH cannot be fully mapped by this procedure. The false-positive rate of stem detection was estimated to be 3.9% (Table 2).

We compared the spatial patterns of ground-measured and TLS-detected stems. A total of 85% of the ground-inventoried stems  $\geq 10$  cm DBH (5104 out of 6027) were identified in the TLS-derived stem map (Fig. 6). The comparison also revealed the existence of geolocation biases in

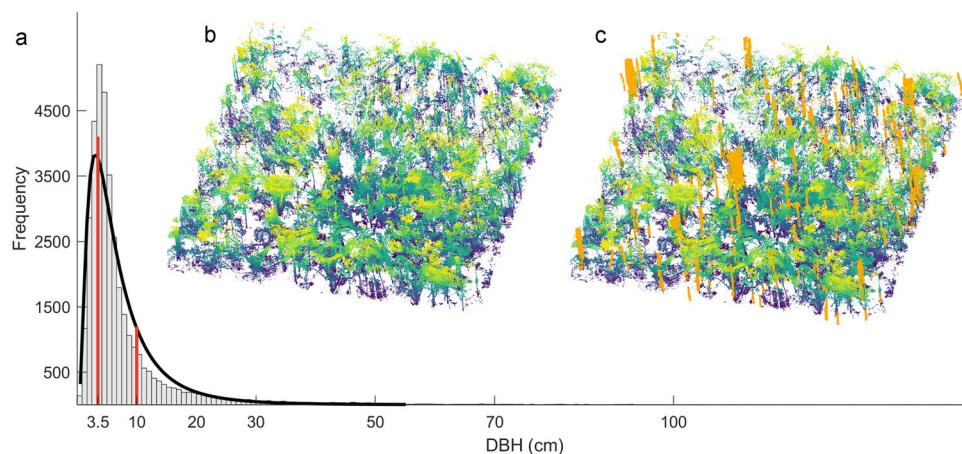


**Fig. 5** TLS detection of tree stems. **a** A histogram shows the DBH distribution of the detected stems with DBH calculated using the “xy-range” approach (see Fig. 3a). The black line is a fit of a log-normal distribution. The red lines mark the peak of the log-normal distribu-

tion (3.5 cm) and the 10-cm threshold. **b** Forest point cloud colored in a blue-yellow color gradient based on the  $z$ -values of the points. **c** Same as **b**, but with the TLS-detected stems indicated in orange

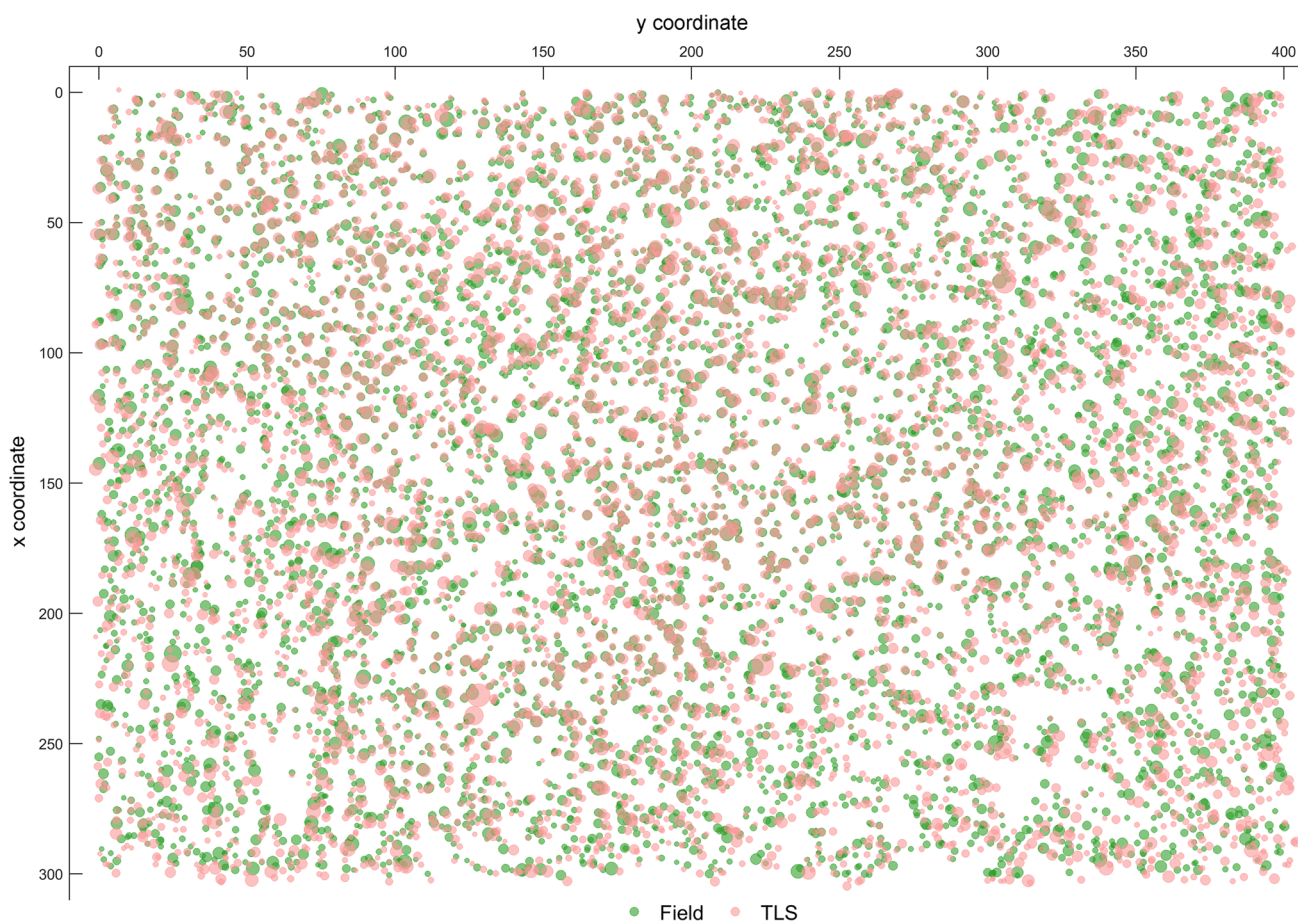
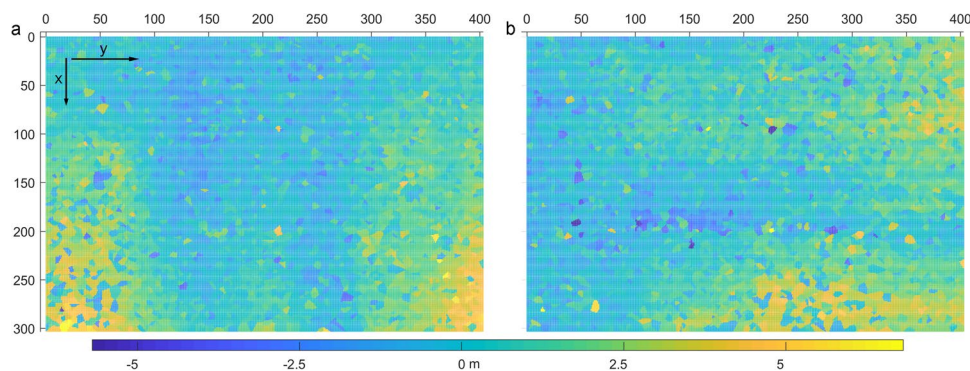


**Fig. 6** Spatial location of 5104 TLS-detected stems (light pink) and ground-censused stems (green). Circle size is proportional to tree size, and only trees  $\geq 10$  cm DBH were mapped

**Fig. 7** Bias in the geolocation of ground-censused stems: along the  $x$  axis (a) and along the  $y$  axis (b). This bias was inferred from 5104 pairwise differences of geolocations (see Fig. 6) and further interpolated across the entire plot



the position of ground-censused trees (Fig. 6). The biases in both the horizontal coordinates of ground-positioned stems were generally lower than 6 m, with a maximum value of 6.8 m (Fig. 7).

TLS-inferred DBHs, as calculated using the “xy-range” approach, correlated strongly with field-recorded values ( $R^2$  of 0.87), with an RMSE of  $\sim 6$  cm, although the procedure over-estimated DBH for a few large trees (Fig. 8a).

The semi-automatic approach largely improved the accuracy of DBH estimation ( $\sim 3$  cm RMSE; Fig. 8b). It also reduced the bias in large DBH values ( $\sim 7$  cm RMSE; Fig. 8c). However, for three large stems, all three with huge buttresses, their estimated DBHs still differed with field recorded values by as much as 20 cm; manual verification of the point cloud suggests possible errors in the field recorded DBHs of these three large trees.

**Fig. 8** Comparison between ground-measured and TLS-estimated DBH. **a** TLS-based versus field measured DBH for 5104 stems, with the TLS-based DBHs estimated using the “xy-range” approach (Fig. 3a). **b** TLS-based versus field measured DBHs for five hundred randomly selected stems, with the TLS-based DBHs calculated using a semi-automatic approach shown in Fig. 3b and 3c. **c** TLS-based versus field measured DBHs for large stems (above 1 m DBH as initially estimated by the “xy-range” approach). TLS-based DBHs were still calculated using the semi-automatic approach but every 1 m along the z axis up to 13 m, and the best match with field values was used here

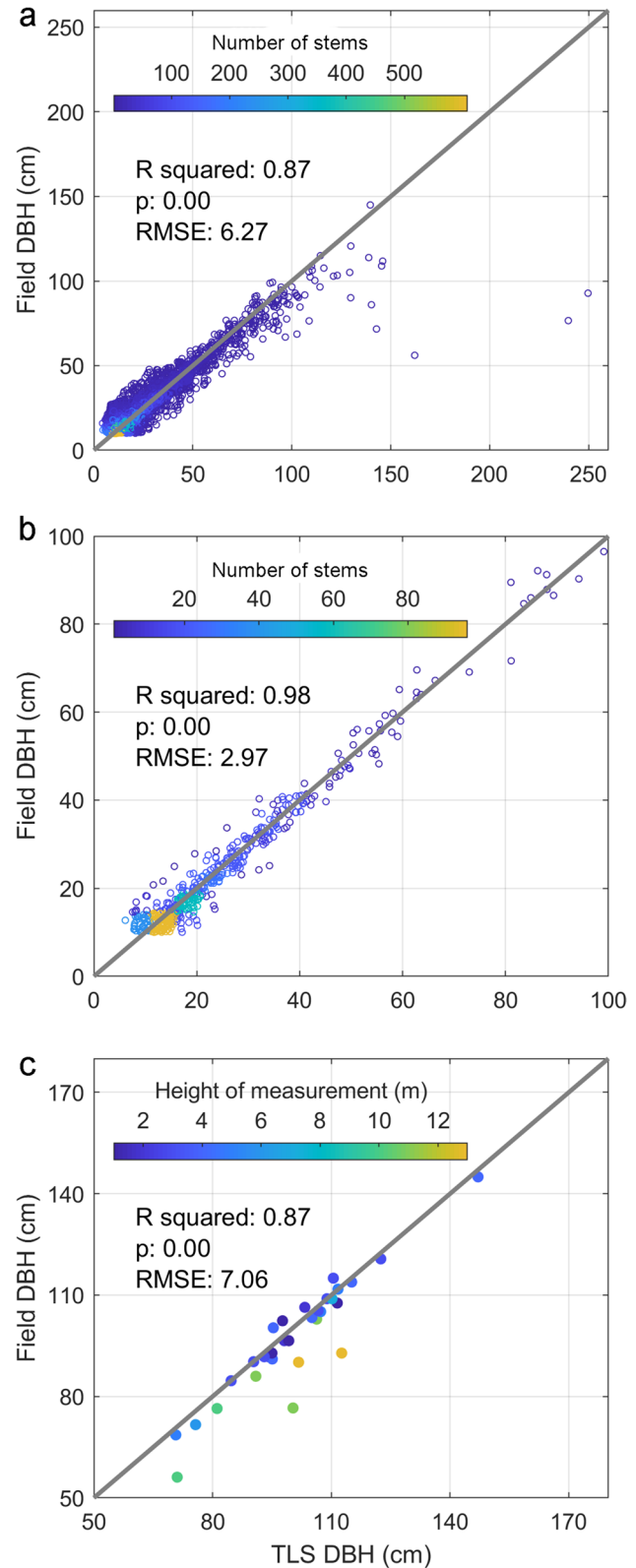
## 4 Discussion

### 4.1 Stem mapping in rainforests

One hectare of tropical rainforest can have 300–1000 trees  $\geq 10$  cm in DBH (DeWalt & Chave 2004). If all individuals  $\geq 1$  cm DBH are considered, these numbers can be up to 10 times higher (Condit et al. 1999). The initial census of a typical 1-ha plot of tropical rainforest for all stems  $\geq 10$  cm DBH represents a significant investment: based on expert knowledge (Duncanson et al. 2021), it requires ca. 75 person-days and costs ca. 18 k€, including direct costs (such as travel, labor cost, and fieldwork) and indirect costs (mainly manpower for quality assessment, botanical expertise, and data management). Less than half of this investment is in actual fieldwork. These figures match well with inventories in French Guiana forests, and the establishment of the 12-ha permanent plot at Nouragues has required an estimated 900 person-days. The investment increases dramatically if small-sized trees  $< 10$  cm DBH are to be surveyed (Hubbell 2001).

Lightweight TLS is a promising, companion solution to classic inventories. One lightweight laser scanner costs around 22 k€ (Leica Cyclone Register 360 software included), which is much cheaper than large TLS systems such as the RIEGL VZ-400. The delivery of a TLS-derived stem map required ca. 10 person-days of fieldwork per hectare (two or three persons achieving 1 ha within 3 or 4 days; Text 1 in the Appendix) and less than four person-days of subsequent data processing (including the time cost of scan co-registration, subsampling, and stem detection). Importantly, TLS data allow the detection of small-sized trees in the range 4–10 cm DBH.

The above comparison of the cost of TLS-based stem mapping and classic field inventory shows that TLS, despite faster mapping, remains a relatively expensive option in complex forest settings such as tropical forests. However, given the advances in this technology, it is possible that costs will further decline in the future. For instance, handheld TLS devices could avoid the need to co-register the TLS scenes, thus avoiding the need of displacing the targets, which currently represents about half of the workload. TLS technology obviously cannot replace manual field inventories: trees need to be tagged physically, TLS systems cannot



identify tree species, and it remains unrealistic to correctly detect all small stems ( $> 1$  cm DBH) from TLS data. Rather, the present study shows that TLS can be used to reduce the

investments of classic inventories, by providing high-accuracy geolocations of many trees in a plot.

## 4.2 Stem mapping with TLS

Cylinder fitting is a classical method to detect stems from the point cloud data, but the stem points of small trees usually do not conform to a cylindrical shape. Thus, a new method to detect tropical stems from point cloud data was developed. The method detected ~3000 stems per hectare in large old-growth tropical forest plots. Most tropical stems with a DBH as small as 4 cm can be detected (Fig. 5). The method has four main parameters, including one for identifying ground points and three for mapping stems.

To separate ground points from vegetation points, the “lasground routine” as implemented in the “lastools” software has been widely used (Korzeniowska et al. 2014). However, “lasground” was initially designed for airborne Lidar. Although recently upgraded for processing TLS data, we found that the output from “lasground” falsely included some vegetation points when applied to our data (Fig. 9a in the Appendix). We therefore designed a filter by calculating the minimum height difference ( $z$ -diff) between each point and its neighbors in the  $xy$ -dimension. True ground points will have a low  $z$ -diff in contrast with vegetation points (Fig. 9 in the Appendix). By thresholding the  $z$ -diff using a histogram, true ground points can be separated from the vegetation points. In our case, we found a natural threshold of around 20 cm (Fig. 9c in the Appendix). However, we set the threshold at 50 cm to check whether woody debris, an important component of the tropical carbon cycle, can be detected. The results (Fig. 4) indicated the capability of our approach to detect woody debris, shedding light on using lightweight TLS to study the structure and volume of woody debris in tropical rainforests.

We then calculated the surface normal of each point. Stem points have horizontal surface normals, unlike most leaf points, so we could remove many leaf points based on this consideration. To further remove leaf points, we noticed that stem points usually have neighboring stem points above or below, or both, but leaf points do not. Based on this consideration, we designed a “tube filter” that checks whether potential stem points exist continuously along the  $z$  axis. The filter was applied on each height layer with a vertical span of 50 cm. It was less challenging and less computer intensive to detect leaning or insufficiently scanned stems with a 50-cm layer than using the 350-cm vertical range. The horizontal dimension of the tube was set to 10 cm: this threshold was chosen because most trees grow at least 10 cm away from neighboring trees. We also tested the sensitivity of the “tube filter” using a 15-cm tube in a subplot (1 ha in area), which showed little difference in the number of detected stems (Fig. 12 in the Appendix).

After filtering, the stem points were segmented into individual components distant horizontally by at least 10 cm. Here, a larger distance threshold would produce less stem-like features (under-segmentation) and a smaller distance more “stems” (over-segmentation). For the tropical forests in our study, the 10-cm threshold provided satisfying accuracy with ~6% under-segmentation errors which can be largely corrected by DBSCAN (Fig. 10a in the Appendix).

Some of the segmented vertical features were not true stems but rather vertical branches. We therefore used the vertical span of the vertical feature to filter out “short” features which are presumed to be branches. The lower the threshold, the more vertical features can be identified, but possibly including more false stems (Fig. 13 in the Appendix). To be conservative, we set a high threshold at 1 m for stems detected from the 1.5–4-m height layers, and 0.8 m for those detected from the 0.5–1.5-m height layers. These two values generated low false-positive errors in rainforests (3.9%; Table 2).

The 3.9% false-positive error rate obtained here, already low, could potentially be further reduced. Most of the false-positive stems have points from only two of the seven height layers between 0.5 and 4 m (Fig. 11c in the Appendix), thus could be detected by setting a threshold in the number of height layers of a stem. Further work will focus on reducing the false-positive error rate, omission errors, and over-segmentation errors of large stems (Fig. 11 in the Appendix). Efforts will also be made to detect more accurately multi-stemmed trees, forked stems, and palm trees which have clustered and angled leaflets.

## 4.3 Comparison with ground inventory

Comparing the stem map with ground mapping and measurement of trees  $\geq 10$  cm in DBH showed promising results (Fig. 6). We found that 85% of the ground-inventoried stems were identified in the TLS-derived stem map. This is similar to the 86% stem detection rate reported by Calders et al. (2018), for 6 ha scanned in Wytham Woods, UK, using a Riegl VZ 400 TLS. The 15% omission error can be explained by two facts. First, there is a 2-year time lag between the TLS scan (in 2019) and the field inventory (in 2017). Tree-fall events during the 2 years can contribute to the mismatch. Another important factor is the occlusion effect (Wilkes et al. 2017), i.e., some stems were occluded by others and thus were not, or insufficiently, scanned. The occlusion effect can be reduced by using a denser scan grid (e.g., 10 × 10 m rather than 20 × 20 m), but at the cost of lower survey cost-efficiency. Most small trees with a DBH < 4 cm were under-detected (Fig. 5), possibly because they were not well-scanned due to their small size and the 20 × 20 m scanning strategy.

By comparing the stem locations between TLS-derived and field inventoried stem maps, we found significant biases in the locations of ground-positioned trees. This suggests that geolocation in rainforest inventories could be error prone even though these inventories have been established decades ago and re-censused frequently. It is likely that structurally complex temperate forests have the same type of geolocation bias. The larger the plots are, or the larger their terrain variability, the more severe biases in tree positions could be. TLS mapping crucially helps reducing this bias. This has implications for checking and correcting (if any) the potential bias in tree positions in large forest plots currently in operation in global forests (Anderson-Teixeira et al., 2015).

#### 4.4 DBH estimation and uncertainty

We used two methods to estimate the diameter of trees. The first is the so-called “xy-range” approach, which automatically estimated stem diameters once stems were detected. It used the stem points with a height above the ground < 4 m as input, thus over-estimates the DBH for stems with buttresses or stilt roots. It also under-estimates the DBH for insufficiently scanned stems. The uncertainty of this approach was around 6 cm (Fig. 8a). We explored other methods such as circle fitting techniques (Pueschel et al. 2013), but found no single best approach to estimate DBH accurately and automatically for all trees with varying stem shapes and scan qualities. For small trees, the stem points can be too few to be circle-fitted. For partially scanned stems, it is better to visually verify whether a circle can be fitted to the stem points and whether the fitted circle is reasonable. For large, irregularly shaped stems with buttresses (such as the case of *Swartzia polyphylla* DC), neither our “xy-range” approach nor the commonly used circle fitting can accurately capture their realistic trunk shapes. The “xy-range” approach, although not perfect, remains the most efficient for automatic estimation of DBH.

To achieve better accuracy, we used a semi-automatic approach. We visually checked the shape and quality of the stem points to choose the most appropriate method for DBH estimation (Fig. 3b, 3c). The accuracy largely increased compared to the “xy-range” approach (Fig. 8b), but three very large stems still had errors of ~20 cm in their estimated DBHs (Fig. 8c). These included the largest tree in the plot, a *Pseudopiptadenia suaveolens* (Miq.) J.W.Grimes (Fabaceae, Mimosoideae), with large buttresses, and a *Pradosia cochlearia* (Lecomte) T.D. Pennington (Sapotaceae), another famously buttressed tree species in French Guiana, known for its fruit-bearing stems. The third large tree was a *Couratari guianensis* (Aubl.), in the Brazil-nut family (Lecythidaceae), known in French Guiana as “mahot cigare” and in Brazil as “tauari,” which also generally has large buttresses.

Because it was difficult to set up a ladder around the huge buttresses, their DBHs were estimated in the field using a camera. Thus, we presume that the mismatch between TLS estimates and field estimates might be due to an error in the latter. Indeed, we extracted the raw stem point cloud for all three stems and carefully explored what would be the most likely value of the stem trunk diameter: after this manual check, a large discrepancy persisted, pointing again to the issue in DBH measurements for the three trees. This shows the advantage of TLS in estimating the size of the largest trees in a plot (Momo Takoudjou et al. 2018).

In this study, we focused on DBH because it is a cornerstone metric in forest inventories. However, as pointed out by Newnham et al. (2015), TLS provides a much richer 3D information than just a DBH. Volume calculation for tree stems could help infer their biomass (Fig. 14 in the Appendix; Calders et al. 2015; Disney et al. 2018), but this might require TLS instruments with a longer range to reach tree tops. For an assessment of simpler forest structure metrics such as DBH, lightweight lower-cost scanners such as the BLK360 or the Canopy Biomass Lidar (CBL, Paynter et al. 2016) provide a rapid and cost-effective solution and can easily be deployed in remote or inaccessible areas (Calders et al., 2020).

For the present analysis, we subsampled the point cloud prior to stem detection (Sect. 2.3). We found that this was not a major cause of the uncertainties in the DBH estimation (Fig. 15 in the Appendix). As discussed above, insufficient scanning (e.g., occlusion effects) influenced the accuracy of the estimated DBH to a much larger extent than subsampling. Thus, DBH estimation could be largely improved with a finer-resolution scan grid (e.g., 10 × 10 m rather than 20 × 20 m). However, there is a balance between point quality and scan efficiency with the BLK360 scanners. Setting up the targets in the field every 20 m was time consuming, and a 10-m grid would have multiplied the effort by a factor of four (Text 1 in the Appendix). Future handheld and backpack TLS systems might be able to achieve even higher scan quality while reducing working time, although currently few (if any) have been tested over large areas in tropical rainforests.

## 5 Conclusion

Using a lightweight terrestrial laser scanning technology, combined with a newly developed stem mapping procedure, we scanned a 12-ha plot of rainforest, created a high-resolution DTM (20 × 20 cm), and mapped 36,422 stems from the acquired point cloud. These results will hopefully advance the use of TLS in stem mapping in tropical rainforests. The stem mapping procedure is poised to considerably facilitate the establishment of large forest plots in rainforests, providing accurate positions of a massive number of trees while

reducing workload. Our study focused on rainforests, but the stem mapping procedure presented here could also be useful for temperate forests having a similarly complex forest structure. We used a BLK360 instrument, but lightweight terrestrial laser scanners are rapidly developing and purchasing costs are decreasing (Newnham et al. 2015). Therefore, the proposed stem mapping procedure could soon become of standard use even in complex forest environments such as mature rainforests and temperate broadleaf forests. Processing advances should further improve stem mapping. Finally, TLS-derived data could be useful for other applications, such as the calculation of coarse woody debris volume, stem volume, and trunk tapering (Cushman et al. 2021).

**Supplementary Information** The online version contains supplementary material available at <https://doi.org/10.1007/s13595-021-01113-9>.

**Acknowledgements** The authors thank people from the Nouragues station (Patrick Chatelet, Florian Jeanne, Bran Leplat, and Elodie Courtois) for help and support to the scan campaign. The authors also thank Emmanuel Vigier, Nino Page, and Emmanuel De Mil for their help with data collection in the rainforest.

**Funding** This work has benefitted from an “Investissement d’Avenir” grant managed by Agence Nationale de la Recherche (AnaEE France ANR-11-INBS-0001; CEBA, ref. ANR-10-LABX-25-01), the CNRS Nouragues station, and a CNES postdoctoral fellowship granted to S.T. Data and code availability.

The datasets generated by this study and data processing codes have been made publicly available at [\[github.com/TonySI/BLK360\\_TLS\]](https://github.com/TonySI/BLK360_TLS).

## Declarations

**Ethics approval** The authors declare that they obtained the approval of The Scientific Committee of the Nouragues Research Station for conducting the study in Nouragues Nature Reserve, French Guiana. **Consent to participate** Not applicable

**Consent for publication** All authors gave their informed consent to this publication and its content.

**Conflict of interest** The authors declare no competing interest. Contribution of the co-authors.

Conceptualization: JC; methodology: ST, NL, FJF, and JC; formal analysis and investigation: ST, NL, FJF, EPR, and LP; writing and original draft preparation: ST; writing, review, and editing: ST, NL, KC, FJF, EPR, LP, and JC; funding acquisition: JC.

## References

- Anderson-Teixeira KJ, Davies SJ, Bennett AC, Gonzalez-Akre EB, Muller-Landau HC, Joseph Wright S, Abu Salim K, Almeyda Zambrano AM, Alonso A, Baltzer JL, Basset Y (2015) CTFSS-Forest GEO: a worldwide network monitoring forests in an era of global change. *Glob Change Biol* 21:528–549
- Bauwens S, Bartholomeus H, Calders K, Lejeune P (2016) Forest inventory with terrestrial LiDAR: a comparison of static and hand-held mobile laser scanning. *Forests* 7:127
- Brede B., Calders, K., Lau, A., Raunonen, P., Bartholomeus, H. M., Herold, M., Kooistra, L., 2019. Non-destructive tree volume estimation through quantitative structure modelling: comparing UAV laser scanning with terrestrial LIDAR. *Remote Sens. Environ.* 233, 111355.
- Brede B, Lau A, Bartholomeus HM, Kooistra L (2017) Comparing RIEGL RiCOPTER UAV LiDAR derived canopy height and DBH with terrestrial LiDAR. *Sensors* 17:2371
- Brienen RJ, Phillips OL, Feldpausch TR, Gloor E, Baker TR, Lloyd J, Lopez-Gonzalez G, Monteagudo-Mendoza A, Malhi Y, Lewis SL, Martinez RV (2015) Long-term decline of the Amazon carbon sink. *Nature* 519:344–348
- Burt A, Disney M, Calders K (2019) Extracting individual trees from lidar point clouds using treeSeg. *Methods Ecol Evol* 10:438–445
- Calders K, Newnham G, Burt A, Murphy S, Raunonen P, Herold M, Culvenor D, Avitabile V, Disney M, Armston J, Kaasalainen M (2015) Nondestructive estimates of above-ground biomass using terrestrial laser scanning. *Methods Ecol Evol* 6:198–208
- Calders K, Origo N, Burt A, Disney M, Nightingale J, Raunonen P, Åkerblom M, Malhi Y, Lewis P (2018) Realistic forest stand reconstruction from terrestrial LiDAR for radiative transfer modelling. *Remote Sens* 10:933
- Calders K, Adams J, Armston J, Bartholomeus H, Bauwens S, Bentley LP, Chave J, Danson FM, Demol M, Disney M, Gaulton R, Krishna Moorthy SM, Levick SR, Saarinen N, Schaaf C, Stovall A, Terryn L, Wilkes P, Verbeeck H (2020) Terrestrial laser scanning in forest ecology: expanding the horizon. *Remote Sens Environ* 251:1121022
- Chave J, Davies SJ, Phillips OL, Lewis SL, Sist P, Schepaschenko D, Armston J, Baker TR, Coomes D, Disney M, Duncanson L (2019) Ground data are essential for biomass remote sensing missions. *Surv Geophys* 40:863–880
- Chave J, Olivier J, Bongers F, Châtelet P, Forget PM, van der Meer P, Norden N, Riéra B, Charles-Dominique P (2008) Above-ground biomass and productivity in a rain forest of eastern South America. *J Trop Ecol* 24:355–366
- Clark, D. B., Clark, D. A., Oberbauer, S. F., Kellner, J. R., 2017. Multi-decadal stability in tropical rain forest structure and dynamics across an old-growth landscape. *PLoS one*, 12.
- Condit R (1998) Tropical forest census plots. Springer Verlag, Berlin
- Condit R, Ashton PS, Manokaran N, LaFrankie JV, Hubbell SP, Foster RB (1999) Dynamics of the forest communities at Pasoh and Barro Colorado: comparing two 50-ha plots. *Philos Trans R Soc B* 354:1739–1748
- Cushman KC, Bunyavejchewin S, Cárdenas D, Condit R, Davies SJ, Duque Á, Hubbell SP, Kiratiprayoon S, Lum SKY, Muller-Landau HC (2021) Variation in trunk taper of buttressed trees within and among five lowland tropical forests. *Biotropica* 00:1–12. <https://doi.org/10.1111/btp.12994>
- DeWalt SJ, Chave J (2004) Structure and biomass of four lowland Neotropical forests. *Biotropica* 36:7–19
- Disney M (2019) Terrestrial LiDAR: a three-dimensional revolution in how we look at trees. *New Phytol* 222:1736–1741
- Disney M, Burt A, Calders K, Schaaf C, Stovall A (2019) Innovations in ground and airborne technologies as reference and for training and validation: terrestrial laser scanning (TLS). *Surv Geophys* 40:937–958
- Disney MI, Boni Vicari M, Burt A, Calders K, Lewis SL, Raunonen P, Wilkes P (2018) Weighing trees with lasers: advances, challenges and opportunities. *Interface Focus* 8:20170048
- Duncanson L et al (2021). Aboveground Woody Biomass Product Validation Good Practices Protocol. <https://doi.org/10.5067/doc/ceoswgcv/lpv/agg.001>
- Ester, M., Kriegel, H. P., Sander, J., Xu, X., 1996. A density-based algorithm for discovering clusters in large spatial databases with noise. In *Kdd* (Vol. 96, No. 34, pp. 226–231).

- Gonzalez de Tanago J, Lau A, Bartholomeus H, Herold M, Avitabile V, Raumonon P, Martius C, Goodman RC, Disney M, Manuri S, Burt A (2018) Estimation of above-ground biomass of large tropical trees with terrestrial LiDAR. *Methods Ecol Evol* 9(2):223–234
- Hubbell SP (2001) A unified neutral theory of biodiversity and biogeography. Princeton University Press, Princeton NJ
- Korzeniowska K, Pfeifer N, Mandlbürger G, Lugmayr A (2014) Experimental evaluation of ALS point cloud ground extraction tools over different terrain slope and land-cover types. *Int J Remote Sens* 35:4673–4697
- Lau A, Martius C, Bartholomeus H, Shenkin A, Jackson T, Malhi Y, Herold M, Bentley LP (2019) Estimating architecture-based metabolic scaling exponents of tropical trees using terrestrial LiDAR and 3D modelling. *For Ecol Manag* 439:132–145
- Liang X, Hyyppä J, Kaartinen H, Lehtomäki M, Pyörälä J, Pfeifer N, Holopainen M, Broly G, Francesco P, Hackenberg J, Huang H (2018) International benchmarking of terrestrial laser scanning approaches for forest inventories. *ISPRS J Photogramm Remote Sens* 144:137–179
- Luck L, Hutley LB, Calders K, Levick SR (2020) Exploring the variability of tropical savanna tree structural allometry with terrestrial laser scanning. *Remote Sens* 12(23):3893
- Maas HG, Bienert A, Scheller S, Keane E (2008) Automatic forest inventory parameter determination from terrestrial laser scanner data. *Int J Remote Sens* 29:1579–1593
- Malhi Y, Jackson T, Patrick Bentley L, Lau A, Shenkin A, Herold M, Calders K, Bartholomeus H, Disney MI (2018) New perspectives on the ecology of tree structure and tree communities through terrestrial laser scanning. *Interface Focus* 8:20170052
- Martin-Ducup, O., Mofack, G. I., Wang, D., Raumonon, P., Ploton, P., Sonké, B., Barbier, B., Coutron, P., Pélissier, R., 2021. Evaluation of automated pipelines for tree and plot metric estimation from TLS data in tropical forest areas. *Annals of Botany*. mcab051, doi.org/https://doi.org/10.1093/aob/mcab051
- Momo Takoudjou S, Ploton P, Sonké B, Hackenberg J, Griffon S, De Coligny F, Kamdem NG, Libalah M, Mofack GI, Le Moguédec G, Pélissier R (2018) Using terrestrial laser scanning data to estimate large tropical trees biomass and calibrate allometric models: a comparison with traditional destructive approach. *Methods Ecol Evol* 9(4):905–916
- Newnham GJ, Armston JD, Calders K, Disney MI, Lovell JL, Schaaf CB, Strahler AH, Danson FM (2015) Terrestrial laser scanning for plot-scale forest measurement. *Curr For Rep* 1(4):239–251
- Pan Y, Birdsey RA, Fang J, Houghton R, Kauppi PE, Kurz WA, Phillips OL, Shvidenko A, Lewis SL, Canadell JG, Ciais P (2011) A large and persistent carbon sink in the world's forests. *Science* 333:988–993
- Paynter I, Saenz E, Genest D, Peri F, Erb A, Li Z, Wiggin K, Muir J, Raumonon P, Schaaf ES, Strahler A (2016) Observing ecosystems with lightweight, rapid-scanning terrestrial lidar scanners. *Remote Sens Ecol Conserv* 2:174–189
- Phillips, O. L., Baker, T. R., Brien, R., Feldpausch, T. R., 2010. Field manual for plot establishment and remeasurement.
- Pueschel P, Newnham G, Rock G, Udelhoven T, Werner W, Hill J (2013) The influence of scan mode and circle fitting on tree stem detection, stem diameter and volume extraction from terrestrial laser scans. *ISPRS J Photogramm Remote Sens* 77:44–56
- Qian C, Liu H, Tang J, Chen Y, Kaartinen H, Kukko A, Zhu L, Liang X, Chen L, Hyyppä J (2017) An integrated GNSS/INS/LiDAR-SLAM positioning method for highly accurate forest stem mapping. *Remote Sens* 9:3
- Raumonon P, Kaasalainen M, Åkerblom M, Kaasalainen S, Kaartinen H, Vastaranta M, Holopainen M, Disney M, Lewis P (2013) Fast automatic precision tree models from terrestrial laser scanner data. *Remote Sens* 5:491–520
- Tao S, Wu F, Guo Q, Wang Y, Li W, Xue B, Hu X, Li P, Tian D, Li C, Yao H (2015) Segmenting tree crowns from terrestrial and mobile LiDAR data by exploring ecological theories. *ISPRS J Photogramm Remote Sens* 110:66–76
- Visser MD, Bruijning M, Wright SJ, Muller-Landau HC, Jongejans E, Comita LS, De Kroon H (2016) Functional traits as predictors of vital rates across the life cycle of tropical trees. *Funct Ecol* 30:168–180
- Yao T, Yang X, Zhao F, Wang Z, Zhang Q, Jupp D, Lovell J, Culvenor D, Newnham G, Ni-Meister W, Schaaf C (2011) Measuring forest structure and biomass in New England forest stands using Echidna ground-based lidar. *Remote Sens Environ* 115:2965–2974
- Wilkes P, Lau A, Disney M, Calders K, Burt A, de Tanago JG, Bartholomeus H, Brede B, Herold M (2017) Data acquisition considerations for terrestrial laser scanning of forest plots. *Remote Sens Environ* 196:140–153

**Publisher's Note** Springer Nature remains neutral with regard to jurisdictional claims in published maps and institutional affiliations.